PROCEEDINGS OF SCIENCE

The Effect of Our Cosmic Neighborhood's Magnetic Field on UHECR Propagation

V. Pelgrims [a,*] **M. Unger** [b,c] **and I. C. Mariş** [a]

[a] *Université Libre de Bruxelles, Science Faculty, CP230, B-1050 Brussels, Belgium*

[b] *Institut für Astroteilchenphysik, Karlsruher Institut für Technologie, Karlsruhe 76344, Germany*

[c] *Institutt for fysikk, Norwegian University of Science and Technology (NTNU), Trondheim, Norway*

E-mail: vincent.pelgrims@ulb.be, michael.unger@kit.edu, ioana.maris@ulb.be

Although individual small-scale magnetized structures in our Galaxy do not have a significant impact on the propagation of UHECRs of energy greater than 1 EeV, they have the potential to influence our reconstruction of the large-scale magnetic field commonly derived from synchrotron and Faraday rotation data. In this context, the Local Bubble - a cavity of hot gas surrounded by a thick magnetized shell extending roughly 100 pc around the Sun - is a very important element to take into account. Here, we focus on the effects of including the Local Bubble and its magnetized shell to reconstruct the large-scale Galactic magnetic field and further explore possible consequences for propagation studies of UHECRs. We find that the magnetized shell of the Local Bubble implies a foreground for Galactic magnetic field observables that leads to changes in the characterization of the magnetic field at large scales, leading to changes in backtracking predictions. These changes are of the order of other uncertainties of global Galactic magnetic field models, and therefore a better understanding of the Local Bubble is needed to improve the precision of backtracking of UHECRs through the Galaxy.

39th International Cosmic Ray Conference (ICRC2025)
15–24 July 2025
Geneva, Switzerland

ICRC 2025
The Astroparticle Physics Conference
Geneva July 15-24, 2025

*Speaker

© Copyright owned by the author(s) under the terms of the Creative Commons Attribution-NonCommercial-NoDerivatives 4.0 International License (CC BY-NC-ND 4.0).

PoS(ICRC2025)357

1. Introduction

Knowledge about the three-dimensional (3D) structure of the Galactic magnetic field (GMF) is important to study ultra-high-energy cosmic rays (UHECR) and interpret their data on arrival direction, mass composition, and energy spectrum [1–3]. To gain insight into the general structure and amplitude of the GMF on the kiloparsec scale relevant to the propagation of UHECRs with energies above 1 EeV, observations of Faraday rotation measures (RM) toward extragalactic sources and Galactic synchrotron emission have been usually used. Using forward modeling frameworks, where model predictions are compared to observations, constraints on a variety of 3D models for the GMF have been deduced (see, e.g., [4]). One of the main limitations of this approach is the line-of-sight-integrated nature of the observables, which produces a degeneracy between GMF models and model parameters [5]. In this context, most efforts to model the large-scale GMF have overlooked the fact that the Solar system resides in the Local Bubble (LB). The LB is a cavity with unusually low density of gas, filled with an X-ray emitting plasma, and surrounded by a thick shell of cold (ionized) gas and dust [6–11]. This local cavity has most likely been created by successive supernova explosions that occurred in the past 10 to 15 Myr [12–14]. As for other explosion-induced bubbles in the interstellar medium (ISM), the initial local magnetic field is expected to have been reshaped by supernova explosions. By dragging the frozen-in magnetic field lines with it, the explosion-induced motion of matter deformed and confined the magnetic field lines into the shell of the resulting bubble. This is supported by starlight polarization data which show that the magnetic field in the local ISM does not follow the large-scale GMF pattern and exhibits an increased amplitude in the shell of the LB [15–20]. Although the LB shell has been shown to dominate the dust polarization signal at high-Galactic latitudes ($|b| \geq 60°$) as measured at 353 GHz by the Planck satellite [10, 21], its contribution to the line-of-sight-integrated Faraday RM and polarized synchrotron emission is still little constrained.

Recently, the magnetized shell of the LB has been implemented in an attempt to model the coherent component of the GMF [22]. It was found that the LB contributes substantially to the Faraday RM and polarized synchrotron emission at high-Galactic latitudes and, hence, has an impact on the reconstruction of the large-scale field. Notably, the authors found that, in their model, the addition of the LB shell naturally eliminates the need for a random striated component (or random ordered component) which was introduced to reconcile the amplitudes of the RM and synchrotron predictions [23]. However, the previous study considered a simple spherical model to describe the LB and used a non-solenoidal parametric model to describe the magnetic field in its shell. To improve on this, we recently derived a divergence-free solution for the magnetic field in the thick shell of irregularly-shaped Galactic bubbles [24], assuming uniform initial conditions. This is convenient to model the magnetic field in the LB shell as it is known to be irregular and highly asymmetric, with a radius of about 100 pc in the Galactic plane and of about 300 pc perpendicular to it [10]. Using our analytical model and more realistic shapes for the shell of the LB as determined from 3D dust density map, we considered six possible scenarios to explore the impact of the geometric characterization of the system on the structure of the magnetic field in the shell. We showed that the choice of the shape of the LB shell and the location of the explosion that has led to the formation of the LB are important factors to consider. They are decisive in estimating the contribution of the magnetized LB shell to the synchrotron polarized emission and Faraday RM,

PoS(ICRC2025)357

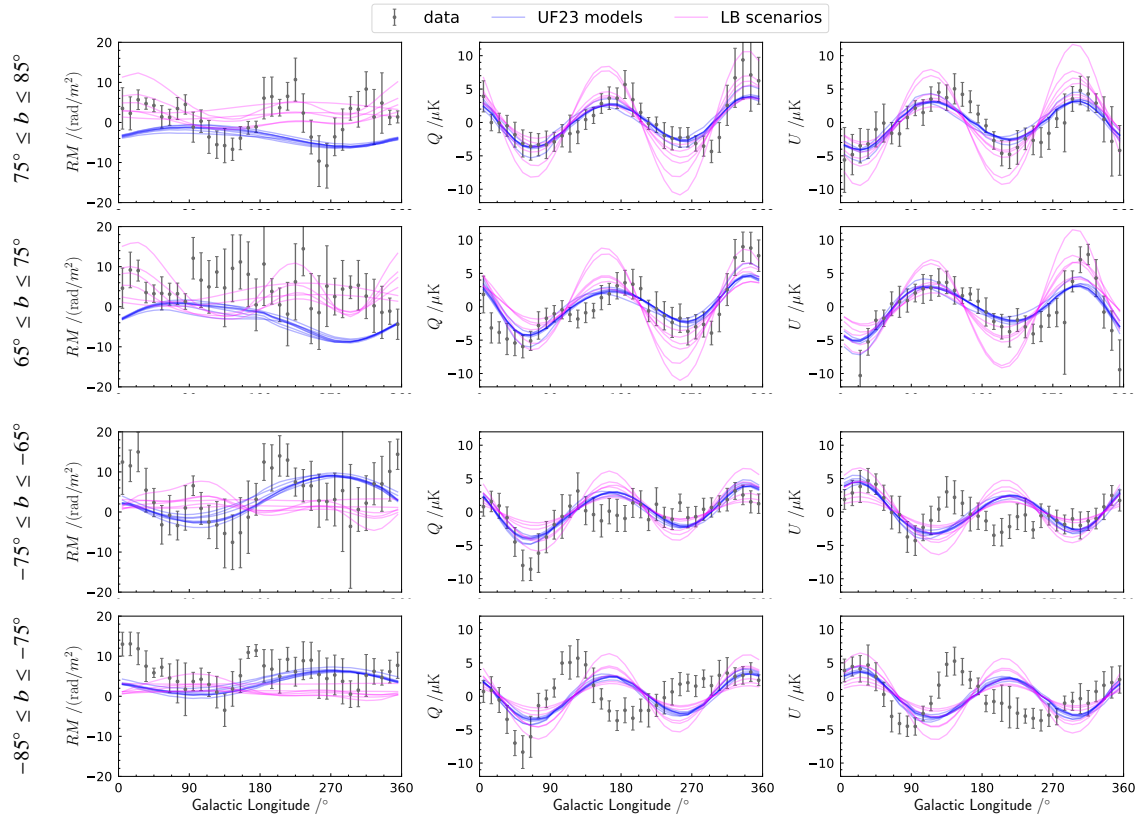

Figure 1: Longitude profiles through the RM, Q, and U (modeled) data (from left to right) for constant latitude stripes of 10° width centered on $b = 80°$, $70°$, $-70°$, $-80°$ (from top to bottom). The profiles are constructed by averaging the data in 10° bins. The blue lines correspond to the height best-fit UF23 models [5] whereas the magenta lines correspond to the six scenarios for the magnetized shell of the LB from [24, 25]. The mean and standard deviation of the data in bins is shown as gray points with symmetric errorbars.

leading to a large variety of large-scale ($\gtrsim 20°$) anisotropies on the sky maps of RM, Q, and U [24]. Interestingly, we found that, even without optimizing the fit to the data, the contribution of the LB shell to the polarized synchrotron signal qualitatively matches the observation at $|b| \gtrsim 65°$. As shown in Figure 1, the match is qualitatively as good as the one obtained from the ensemble of large-scale GMF models proposed in [5] (hereafter UF23). This similarity suggests that the two components (large-scale and LB shell) might compete to reproduce the observations. This may produce biases in current modeling of the large-scale GMF and, hence, in propagation studies of UHECRs. This is what we investigate in this work by adding the magnetized shell of the LB as an additional component to those making the `base` model of the UF23 ensemble.

2. Including the magnetized LB shell into a large-scale GMF model

A model for the magnetized shell of the LB Starting from the induction equation without magnetic diffusion, we obtained the solenoidal solution for the magnetic field in the thick shells of Galactic bubbles that result from supernova explosion [24]. The model assumes a single effective explosion that induces a radial displacement of the ISM matter with respect to the explosion

PoS(ICRC2025)357

center, but not necessarily with spherical symmetry. According to the frozen-in approximation, the magnetic field that is assumed to be initially uniform ($\mathbf{B}^0$) is then deformed, following the displacement of matter. Considering a simple linear model for the matter displacement field, we proposed a solution that is solenoidal by construction and makes it possible to fully describe the magnetic field $\mathbf{B}$ anywhere in the shell of Galactic bubbles from the characterization of the inner and outer surfaces of the bubble shell, the explosion center, and $\mathbf{B}^0$. This model is well suited to exploring the impact of the choice of shell shape and explosion center location on predictions of the LB shell contribution to the Faraday RM and the synchrotron polarized emission. We presented such a study relying on published values for all model parameters, and relying on the inner and outer surfaces of the LB shell as derived from the 3D dust density map of [26]. The longitude profiles shown in Figure 1 (magenta lines) are computed from these model maps for constant latitude stripes of 10° width. In the remainder of this work, we focus on the LB scenario named `DDO`. For this scenario, the inner and outer surfaces of the LB shell are given by $r_{\rm inner}^{\ell_{\rm max}=6}$ and $r_{\rm outer}^{\ell_{\rm max}=6}$ derived from the 3D dust map of [26], and the effective explosion center has heliocentric Cartesian coordinates $(x_c,\, y_c,\, z_c) = (-24.8, -32.6, -23.3)$ pc. The amplitude of the initial magnetic field was fixet at 3 μG and its direction was given by $(l^0,\, b^0) = (73°,\, 17°)$, according to the best-fit values obtained in [10] from modeling the polar regions ($|b| > 60°$) of the polarized dust emission measured at 353 GHz. In this work, we will explore the parameter space for $\mathbf{B}^0$.

A model for the large-scale GMF features To capture the structure of the GMF on large scales ($\gtrsim$ 100 pc), UF23 developed an ensemble of eight parametric models that they constrained by jointly fitting for the Faraday RM and synchrotron Stokes parameters Q and U. In their `base` model, the GMF is made of three main components to describe the coherent part of the GMF. A three-mode grand-design spiral disk field, an explicit toroidal halo, and a coasting X-field with a logistic sigmoid radial dependence, all controlled by $9 + 5 + 5$ parameters. An additional parameter (ξ) controls the amplitude of the striated random component relative to the coherent one.

Including the LB shell in a large-scale GMF model To infer the effects of including the magnetized shell of the LB on the modeling of the large-scale GMF, we proceed as follows. The magnetized Galaxy is simulated using the UF23-`base` model exactly as in UF23 except that, in the volume now encompassed by the LB and its shell, the GMF ($\mathbf{B}$) and the thermal electron density (n_e) are replaced by the values predicted by our analytical model. The volume is centered on the Sun and is defined by the outer surface of the LB shell ($r_{\rm outer}^{\ell_{\rm max}=6}$). Considering only the `DDO` scenario, where the shell geometry and the explosion center are fixed, n_e and $\mathbf{B}$ in the shell of the LB are fully determined by their initial values, ${n_e}^0$ and $\mathbf{B}^0$ respectively. We consider that the cosmic-ray electron (CRE) density is un-altered by the explosion and is given by the value given by the UF23 model. Adopting the values of ${n_e}^0 = 0.015\,{\rm cm}^{-3}$ and considering varying values for $\mathbf{B}^0$, we then synthesize the contributions from the LB shell to the observables, considering 10 equally spaced grid points along each line of sight through the LB shell. These contributions are then added to those corresponding to the outside of the LB and obtained from the UF23-`base` model. We parametrize $\mathbf{B}^0$ with two parameters; one for its amplitude B^0 and one for its initial direction (l^0, b^0) that we discretize using the pixel ID of an HEALPix map with resolution parameter $N_{\rm side} = 4$ [27, 28]. Our baseline model has thus $20 + 2$ independent free parameters that are adjusted to match the

PoS(ICRC2025)357

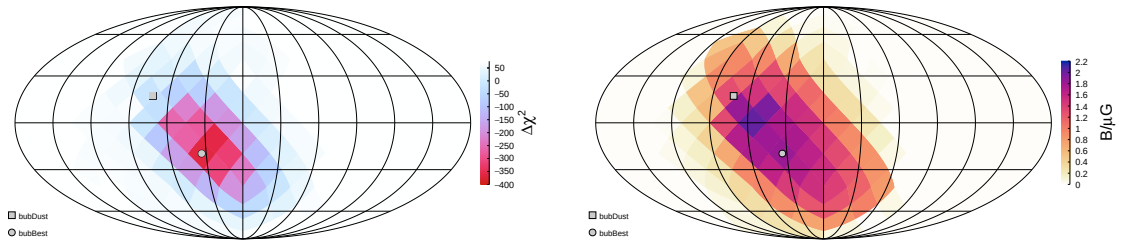

Figure 2: Maps of the $\Delta\chi^2$ (left) and best-fit value for B^0 (right). Maps are in Galactic coordinate system. The direction for the initial magnetic field corresponding to the absolute minimum χ^2 and to the best fit of [10] are marked with a gray circle and square, respectively.

observations.

3. Best-fit results

We follow UF23 to constrain our model and obtain the best-fit parameters, using the same data on Faraday RM and synchrotron Q and U, with the same mask and binned at the same resolution ($N_{\rm side} = 16$) while minimizing the total χ^2. The parameter-space exploration is started independently for every initial-direction pixel and the χ^2 minimization is performed using the MINUIT program [29]. For every discretized (l^0, b^0), we obtain the minimum χ^2 along with the best-fit values for the other $20+1$ model parameters. The absolute minimum χ^2/ndf of this model, which we named `bubBest` is $7561/6498 \approx 1.16$ and is reached for $(l^0, b^0) \approx (34°, -19°)$ with a best-fit $B^0 = 1.8$ μG. This minimum can be compared to the one of $7923/6500$ reached using the original UF23-`base` model. The `bubBest` model leads to a better fit to the polarization data as compared to the UF23-`base` model, with a $\Delta\chi^2 \coloneqq \chi^2_{\rm bubBest} - \chi^2_{\rm base} = -362$. We show the map of $\Delta\chi^2$ in Figure 2 (left) and the corresponding map of the best-fit values for B^0 (right). The best-fit values for the parameters of the large-scale field remain globally unchanged as compared to the UF23-`base` model, except for the poloidal component (X-shape) that shows an almost tripled value for its scale height (z_p parameter in UF23) and a reduction of the striation factor ($\xi \simeq 0.25$ instead of $\simeq 0.35$). In Figure 3 (top panel), we show the contributions to the GMF observables of the different components of our best-fit models (disk, toroidal, poloidal, and LB shell).

In the maps of Figure 2, we also show with a gray square the best-fit direction of $\mathbf{B}^0$ obtained from a fit to the polar Galactic regions of the dust polarized emission in [10]. Fixing $(l^0, b^0) = (73°, 17°)$ from their best-fit leads to a variant of our model that we named `bubDust`. With an achieved minimum χ^2/ndf of $7910/6499$ (with $B^0 = 1.3$ μG), this variant leads to an equally good fit than the UF23-`base` model ($\Delta\chi^2 = -13$). For this variant, the amplitude of the north and south toroidal halo components are increased by about 1 μG while their scale height is reduced by about 1 kpc (z_t in UF23). The striation factor undergoes a similar reduction than in the case of `bubBest`. The contributions to the GMF observables of the different components of this model is shown at the middle panel of Figure 3. A serendipitous alignment of synchrotron Q and U from the LB shell and for large-scale (disk, poloidal and toroidal) components can be observed. This is reminiscent of what was already observed in Figure 1. Further analysis is needed to better understand this alignment, elucidate its origin, and study its implications for GMF modeling.

PoS(ICRC2025)357

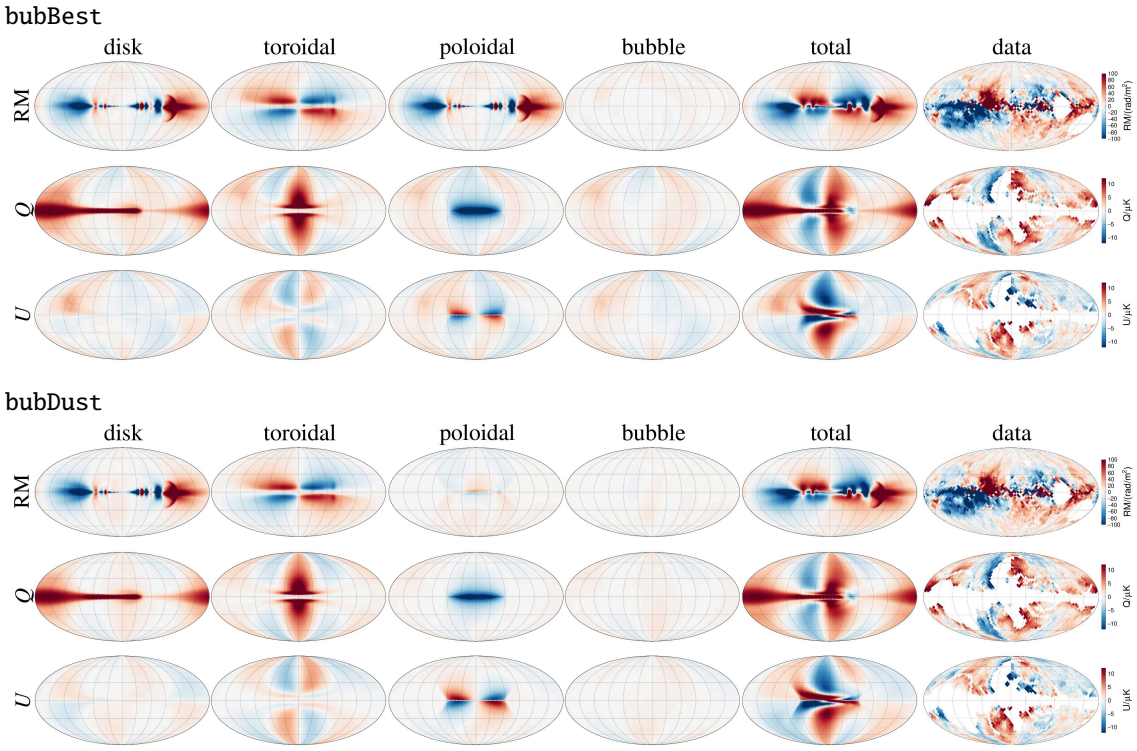

Figure 3: Mollweide projection in Galactic coordinates of the predicted contributions to GMF observables from the different GMF components. The top and bottom panels show the results for the variants named `bubBest` and `bubDust`. In each panel, the predictions for RM, Q, and U are shown from the top to bottom rows. The first four columns show the individual contributions from the disk, toroidal, poloidal and LB shell (left to right), and the fifth and sixth column show the results of the complete model and the data.

Noticing that (*i*) the Q and U signal from the LB shell for the `bubDust` model is well aligned to the one obtained from the large-scale GMF and (*ii*) that the amplitude of the striated random component of the GMF is somewhat suppressed in this model as compared to the original UF23-`base` model, we further consider an additional variant, named `noStria`, where ξ is forced to be zero (in addition to fixing $(l^0, b^0) = (73°, 17°)$). This variant leads to a minimum χ^2/ndf of 7982/6500 for $B^0 = 1.8$ µG. Thus, allowing for a striated random field component leads to a very modest improvement of the fit: $\chi^2_{\text{bubDust}} - \chi^2_{\text{noStria}} = -72$. Interestingly, for the `noStria` variant the amplitude of the north and south toroidal halo components are approximately doubled while the scale height is reduced by half; leading to a toroidal field more compact close to the Galactic plane but leaving the overall integrated magnetic field approximately unchanged.

4. Impact on UHECR backtracking

As just discussed, the inclusion of the magnetized LB shell into the modeling of the GMF induces changes in the best-fit values of the parameters that describe the GMF at the largest scales, relevant to the propagation of UHECRs. To quantify the possible effects that those changes imply in propagation and arrival direction studies, we carry out a first test based on the model variants presented above, together with then ensemble of models presented in UF23. Within each of the 11

PoS(ICRC2025)357

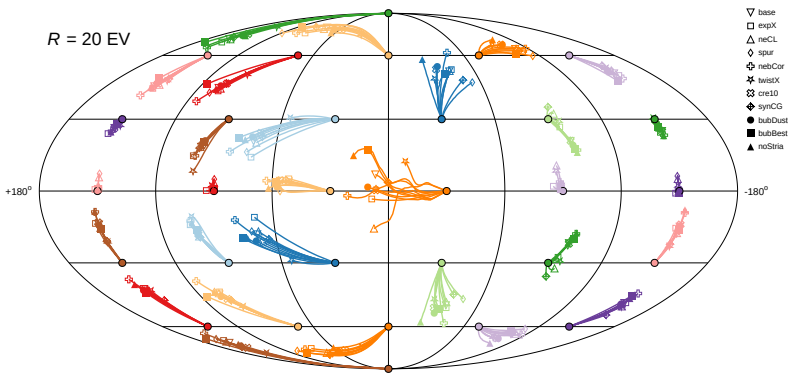

Figure 4: Angular deflections of UHECRs with rigidity of 20 EV for a grid of 32 arrival directions denoted by the filled circles with black edges. The backtracked directions at the edge of the Galaxy are given for the eight UF23 models (open symbols) and the three variations introduced in this work (filled symbols).

models for the GMF, we backpropagate UHECRs with rigidity $R = 20$ EV through the Milky Way, from the Sun location to the edge of the Galaxy. We sample the sky with a small set of 32 arrival direction at Earth.

In Figure 4, we show the arrival directions (filled circles with black contours) and the backtracked directions for the three models introduced in this work (colored filled symbols) and the ensemble of models from UF23 (colored open symbols). The arrival direction and the backtracked directions are connected by lines interpolating the backtracked directions at higher rigidities. Comparing the backtracked directions from our model variants with those of the UF23-`base` (open downward triangles), we see that the inclusion of the LB shell induces a systematic, inhomogeneous shifts, the details of which depend on the specific variant. This suggests that the inclusion of the LB shell might impact the determination of the lensing maps used in search for the sources of UHECRs or preferred source class [30]. In addition, we find that, globally, the differences in UHECR deflections due to changes in the large-scale GMF parameters are of the same order as other uncertainties derived from the ensemble of models in UF23. The somewhat larger differences in backtracked directions obtained for the model of [22] and reported in [31] are therefore probably not solely due to the inclusion of the LB in this GMF model, but rather to other model features.

5. Conclusion

In this work, taking advantage of the recent developments to describe the magnetic field in the shell of the LB, we investigated the impact of including the later to the description of the GMF has on the characterization of the large-scale, regular GMF. We considered variations of the UF23-`base` model in which the volume now encompassed by the LB and its shell is replaced by the dedicated model. We reran the minimization to obtain preliminary best-fit maps of Faraday RM and synchrotron Q and U and derived the best-fit parameters of our models. We found a serendipitous alignment of the predictions for Q and U of global GMF features (disk and halo) and those of the LB shell when the initial orientation of the magnetic field at the location of the LB is taken from a fit to the dust polarization. In this case, the Q and U contributions from the LB shell coherently adds to the emission from the global field and may therefore replace the contribution from the striated random component. This corroborates earlier findings [22]. However, the alignment is somewhat surprising and further dedicated studies will be required to understand it and explore its effects on

PoS(ICRC2025)357

the modeling of the GMF. In parallel, we noticed that adding the magnetized shell of the LB into the modeling of the GMF induces changes in the best-fit values of the model parameters that describe the GMF at large scales. For a small set of arrival directions, we showed that the inclusion of the LB shell induces differences in UHECR deflection angles of up to several degrees, even for rigidities above 20 EV. While the backtracked directions globally remain in the bulk of uncertainties derived from the UF23 ensemble of models, we showed that they depend on the detailed characterization of the magnetic field in the shell of the LB.

This study confirms that the shell of the LB acts as a foreground that needs to be taken into account to model the large-scale GMF from Faraday RM and synchrotron polarization and that accounting for this foreground may impact searches for UHECR sources. To move forward, the magnetic field in the shell of the LB needs to be characterized at best so as to reduce uncertainties in UHECR deflections.

Acknowledgments

VP acknowledges funding from a Marie Curie Action of the European Union (grant agreement No. 101107047).

References

[1] A. Coleman *et al.* *Astropart. Phys.* **149** (2023) 102819.
[2] A. A. Halim *et al.*, [Pierre Auger Coll.] *JCAP* **01** (2024) 022.
[3] G. R. Farrar and M. S. Sutherland *JCAP* **05** (2019) 004.
[4] T. R. Jaffe *Galaxies* **7** no. 2, (2019) 52.
[5] M. Unger and G. R. Farrar *ApJ* **970** no. 1, (2024) 95.
[6] D. P. Cox and R. J. Reynolds *ARAA* **25** (1987) 303–344.
[7] R. Lallement, B. Y. Welsh, J. L. Vergely, F. Crifo, and D. Sfeir *A&A* **411** (2003) 447–464.
[8] W. Liu *et al.* *ApJ* **834** no. 1, (2017) 33.
[9] M. C. H. Yeung, G. Ponti, M. J. Freyberg, K. Dennerl, *et al.* *A&A* **690** (2024) A399.
[10] V. Pelgrims, K. Ferrière, F. Boulanger, R. Lallement, and L. Montier *A&A* **636** (2020) A17.
[11] T. J. O'Neill, C. Zucker, A. A. Goodman, and G. Edenhofer *ApJ* **973** no. 2, (2024) 136.
[12] J. Maíz-Apellániz *ApJL* **560** no. 1, (2001) L83–L86.
[13] D. Breitschwerdt, J. Feige, M. M. Schulreich, M. A. D. Avillez, *et al.* *Nature* **532** no. 7597, (2016) 73–76.
[14] M. M. Schulreich, J. Feige, and D. Breitschwerdt *A&A* **680** (2023) A39.
[15] C. Heiles, "The Magnetic Field Near the Local Bubble," in *IAU Colloq. 166: The Local Bubble and Beyond*, D. Breitschwerdt, M. J. Freyberg, and J. Truemper, eds., vol. 506, pp. 229–238. 1998.
[16] J. L. Leroy *A&A* **346** (1999) 955–960.
[17] B. G. Andersson and S. B. Potter *MNRAS* **356** no. 3, (2005) 1088–1098.
[18] B. G. Andersson and S. B. Potter *ApJL* **640** no. 1, (2006) L51–L54.
[19] G. A. Gontcharov and A. V. Mosenkov *MNRAS* **483** no. 1, (2019) 299–314.
[20] I. Medan and B. G. Andersson *ApJ* **873** no. 1, (2019) 87.
[21] R. Skalidis and V. Pelgrims *A&A* **631** (2019) L11.
[22] A. Korochkin, D. Semikoz, and P. Tinyakov *A&A* **693** (2025) A284.
[23] R. Jansson and G. R. Farrar *ApJ* **757** no. 1, (2012) 14.
[24] V. Pelgrims, M. Unger, and I. C. Mariş *A&A* **695** (2025) A148.
[25] V. Pelgrims, M. Unger, and I. C. Mariş, "Does the Local Bubble bias Galactic magnetic field models used to backtrack UHECRs?," in *7th International Symposium on Ultra High Energy Cosmic Rays*, p. 108. 2025.
[26] R. Lallement, C. Babusiaux, J. L. Vergely, D. Katz, *et al.* *A&A* **625** (2019) A135.
[27] K. M. Górski, E. Hivon, A. J. Banday, B. D. Wandelt, *et al.* *ApJ* **622** no. 2, (2005) 759–771.
[28] A. Zonca, L. Singer, D. Lenz, M. Reinecke, *et al.* *The Journal of Open Source Software* **4** no. 35, (2019) 1298.
[29] F. James and M. Roos *Comput. Phys. Commun.* **10** (1975) 343–367.
[30] T. Bister, G. R. Farrar, and M. Unger *ApJL* **975** no. 1, (2024) L21.
[31] A. Korochkin, D. Semikoz, and P. Tinyakov `arXiv:2501.16158`.

PoS(ICRC2025)357